INTERNATIONAL JOURNAL OF CLIMATOLOGY
Int. J. Climatol. **25**: 713–733 (2005)
Published online in Wiley InterScience (www.interscience.wiley.com). DOI: 10.1002/joc.1156

SOLAR-INDUCED AND INTERNAL CLIMATE VARIABILITY AT DECADAL TIME SCALES

MIHAI DIMA,[a,b]* GERRIT LOHMANN[a,b] and IOANA DIMA[c]
[a] *Department of Geoscience, University of Bremen, Bremen, Germany*
[b] *Alfred Wegener Institute for Polar and Marine Research, Bremerhaven, Germany*
[c] *University of Washington, Seattle, WA, USA*

Received 1 July 2004
Revised 8 December 2004
Accepted 8 December 2004

ABSTRACT

Statistical analyses of long-term instrumental and proxy data emphasize a distinction between two quasi-decadal modes of climate variability. One mode is linked to atmosphere–ocean interactions ('the internal mode') and the other one is associated with the solar sunspots cycle ('the solar mode'). The distinct signatures of these two modes are also detected in a high-resolution sediment core located in the Cariaco basin. In the oceanic surface temperature the internal mode explains about three times more variance than the solar mode. In contrast, the solar mode dominates over the internal mode in the sea-level pressure and upper atmospheric fields. The heterogeneous methods and data sets used in this study underline the distinction between these decadal modes and enable estimation of their relative importance. The distinction between these modes is important for the understanding of climate variability, the recent global warming trend and the interpretation of high-resolution proxy data. Copyright © 2005 Royal Meteorological Society.

KEY WORDS: decadal variability; climate; solar influence; atmosphere–ocean interaction

1. INTRODUCTION

The solar influence on climate variability has been a controversial research problem for a long time (Hoyt and Schatten, 1997; Waple and Bradley, 1999; Mitchell *et al*., 2001). Counting the number of sunspots, periodic signals have been identified in association with the solar forcing, like the ∼11 year Schwabe cycle, the ∼22 year Hayle cycle and the ∼76–90 year Gleissberg cycle (e.g. Hoyt and Schatten, 1997). The connection between the sunspot cycle (hereafter SSC) and the Earth surface was emphasized through modelling studies. Such studies have shown that a decrease of just 0.1% in the solar activity associated with the ∼11 year solar cycle would affect the surface climate through dynamical effects originating in the stratospheric ozone and associated temperature changes (Haigh, 1999; Shindell *et al*., 1999). The established connection between the solar mode and the stratospheric vortex (Labitzke, 2001) may be viewed as a first step in Sun's 'path' towards the surface. Furthermore, changes in the strength of the stratospheric polar vortex affect the variability of the surface fields (Black, 2002), specifically the sea-level pressure (SLP) and the Arctic oscillation (AO) associated variations (Thompson and Wallace, 1998). Since the AO has a strong fingerprint in the North Atlantic area, where it identifies with the more regional North Atlantic oscillation (NAO; Hurrel, 1995), it appears natural to search for a possible solar signature in this region. Another important advantage of investigating the North Atlantic area is the relatively good coverage and quality of the observational data here.

Modes of variability that arise from atmosphere–ocean interactions also have a strong projection onto the climate in the Atlantic area (Grötzner *et al*., 1997). One particular mode of Atlantic climate variability is

* Correspondence to: Mihai Dima, Department of Geoscience, University of Bremen, 28359 Bremen, Germany;
e-mail: dima@palmod.uni-bremen.de

found at decadal time scales (Deser and Blackmon, 1993). The associated sea-surface temperature (SST) signature of this mode is characterized by a North Atlantic tripolar pattern, whereas the corresponding SLP pattern is represented by a basin-scale north–south dipole and midlatitudinal anomalous westerly winds. It has been proposed that this mode results from ocean–atmosphere and tropics–midlatitudes interactions in the North Atlantic basin (Dima *et al*., 2001).

To quantify the solar effects on climate one has to make a distinction between contributions resulting from internal climate variability and those related to other forcings, because the former type of variability may mask the signals coming from the Sun (Rind, 2002). It is the goal of the study to emphasize a distinction between two decadal modes of climate variability of different origins and to estimate their relative importance.

The data and the methods used in this study are presented in Section 2, and the modes identified through statistical analyses of instrumental data are evaluated in Section 3. The modes are also distinguished in upper troposphere reanalysis data (Section 4) and in patterns associated with a high-resolution marine sediment record originating in the southern Caribbean (Section 5). The results are summarized and discussed and conclusions are drawn through the final two sections of the paper.

2. DATA AND METHODS

Unlike previous investigations, where the separation between forced and internal climate variability was emphasised through numerical model experiments (e.g. Hansen and Lacis, 1990; Cubasch *et al*., 1997), the focus here is to identify the characteristic patterns related to solar-induced variability and internal climate variability at decadal time scales, based on analyses of instrumental, reanalysis and reconstructed data sets. In order to compensate for the quality and limited time extension of the data, different types of statistical methods and data are applied in our analyses.

2.1. Data

Instrumental SST data are obtained from the Comprehensive Ocean–Atmosphere Data Set (COADS; da Silva *et al*., 1994). Other SST fields used are derived from the Kaplan *et al*. (1998) data set, which was compiled from an extended version of the COADS (Smith and Reynolds, 2003) and the GISST (Parker *et al*., 1995) data sets. The analysis is concentrated on the North Atlantic Ocean, which, by comparison with other areas, is relatively well covered by direct measurements.

SLP fields are obtained from Trenberth and Paolino (1980) and they partially cover the Northern Hemisphere (15–90 °N). Furthermore, monthly National Centers for Environmental Prediction–National Center for Atmospheric Research (NCEP–NCAR) reanalysis zonal and meridional wind data at 200 hPa (Kalnay *et al*., 1996; Kistler *et al*., 2001) mapped on a global grid are used to calculate the horizontal streamfunction field at that level.

To complete the analysis, a high-resolution time series of marine sediments from the Cariaco basin in the southern Caribbean region is analysed in order to identify its embedded periodic time-components (Black *et al*., 1999). The data set provides a sub-decadal resolved record of Atlantic climate variability. The numbers of individuals per gram of sediment for the planktic foraminifer *Globigerina bulloides* are collected from the Cariaco basin, Venezuela. The record has yearly resolution and exhibits strong decadal to centennial climate variability. The time series most likely reflects variations in the SST, the strength of the trade winds and the position of the intertropical convergence zone. The age model is based on a combination of varve counts (^{210}Pb) and accelerator mass spectrometry (^{14}C) dates.

As a proxy for the sunspot cycle we use the monthly sunspots number time series (McKinnon, 1987). Independent solar data reconstructions by Hoyt and Schatten (1994) and Lean *et al*. (1995) are based on different Sun-related data (the length and amplitude of the ∼11 year Schabe cycle, but also other extra information) and show some phase differences. Since our study is strictly focused on the 11 year cycle, we resume to using the 'raw' number of sunspots to define the 'sunspot time series' in our study. A synthesis of the data sets used in the present study and their characteristics is presented in Table I.

Table I. Characteristics of the data sets used in the present study

Field	Source	Period	Spatial resolution	Temporal resolution
SST (COADS)	Da Silva *et al*. (1994)	1945–89	4° × 4°	Monthly
SST (Kaplan *et al*.)	Kaplan *et al*. (1998)	1856–1991	5° × 5°	Annual
SST (extended COADS)	Smith and Reynolds (2003)	1854–1997	4° × 4°	Annual
SST (GISST)	Parker *et al*. (1995)	1870–1998	2.8° × 2.8°	Annual
SLP (Trenberth and Paolino)	Trenberth and Paolino (1980)	1950–97	5° × 5°	Monthly
Streamfunction (NCEP/NCAR reanalysis)	Kalnay *et al*. (1996), Kistler *et al*. (2001)	1948–98	2.5° × 2.5°	Monthly
Cariaco proxy record	Black *et al*. (1999)	1166–1990	—	Annual
Sunspot number time series	McKinnon (1987)	1700–2000	—	Annual

2.2. *Methods*

Our approach in identifying climatic modes is based on multivariate analyses such as the empirical orthogonal functions (EOFs) and the principal oscillation pattern (POP). For a detailed description of these methods, refer to von Storch and Zwiers (1999). The term 'mode' is used throughout the paper to refer to a set of physical processes that are part of a large-scale coherent spatial structure and that have a quasi-periodic time evolution.

By construction, the EOF method is effective in separating modes with different characteristic spatial patterns. As a complementary approach, the POP method (Hasselmann, 1988; von Storch and Zwiers, 1999) provides modes with distinct spatial structures as well as associated characteristic time scales.

The POP technique is a multivariate method used empirically to infer characteristics of the space–time variations of a complex system in a high-dimensional space. Whereas the EOF method provides only a static description for a mode (the spatial structure at a particular phase and the corresponding time evolution), the POP technique allows the building of a dynamic picture for a mode. A pattern identified through the EOF method may completely change with time, whereas an eigenvector identified through the POP method maintains its structure during its dynamical evolution. The real and imaginary parts of the POP describe different phases in the evolution of the mode. Assuming that a mode shows a quasi-periodic evolution, the imaginary and real structures of a POP may be used to reconstruct the dynamics of a mode over the complete cycle. The evolution of the spatial structure of a POP eigenvector results from the following sequence:

$$\text{Imaginary} \geq \text{Real} \geq -\text{Imaginary} \geq -\text{Real} \tag{1}$$

The significance of a POP identified mode may be inferred using several criteria:

- The percentage of explained variance: a high value of explained variance signals a significant mode, but not necessarily a periodic or stable mode as well.
- The quasi-periodic nature of the time components corresponding to the imaginary and real POP; these indicate that the respective mode is quasi-periodic.
- The time components associated with the imaginary and real parts of a POP are in quadrature (constantly shifted in time); this indicates a standing mode.
- The value of the ratio between the period and the damping time is used to infer the stability and persistence of a mode: when the damping time is comparable to or longer than the period, then this is an indication that the respective mode is stable.

Table II. Technical synthesis of the analyses

Method	Data	Preprocessing	Motivation for preprocessing
POP	SST (COADS)	Detrend 5 year running mean	Remove interannual variability
EOF	SST (several data sets)	Detrend 9–14 year band pass filter	Isolate the decadal time scales
Correlation	Sunspots — SST (Kaplan *et al.* SST)	Detrend 9–14 year band-pass filter	Isolate the decadal time scales
POP	SLP (Trenberth &Paolino)	Detrend 5 year running mean	Remove interannual variability
EOF	Streamfunction (NCEP reanalysis)	9–14 year band-pass filter	Isolate the decadal time scales
SSA	Cariaco record	50 year high-pass filter	Remove multidecadal and longer term variability

The singular spectrum analysis (SSA) technique was applied to identify quasi-periodic components within different time series (Allen and Smith, 1997). The method may be interpreted as sliding a window of chosen width M down a time series, while determining the orthogonal patterns that best capture the variance within the time component.

The statistical significances of estimated correlations are tested using Student t-statistics (von Storch and Zwiers, 1999), under the null hypothesis that there is no real correlation between the two variables considered:

$$t = r[(N_{\text{eff}} - 2)/(1 - r^2)]^{1/2}$$

where r denotes the estimated correlation coefficient between the two variables and N_{eff} is the effective number of degrees of freedom. In order to account for the serial correlation that occurs within the time series, the effective number of degrees of freedom N_{eff} is estimated using the methods of Leith (1973) and Jones (1975):

$$N_{\text{eff}} = N(1 - r_1)/(1 + r_1)$$

where N is the number of samples in each time series and r_1 is the lag-1 autocorrelation coefficient of the time series obtained as a product between deviations of the two variables considered. An overview of the analyses performed in the present study is presented in Table II.

3. MODES IDENTIFIED IN SURFACE FIELDS

3.1. POP analysis of the SST field

The POP method is the first tool used to derive quasi-periodic climate modes. It is applied to the monthly COADS SST field (1945–89) for the North Atlantic region (80 °W–0°, 0–65 °N). Prior to the analysis, the anomalous field was detrended. Because the study is focused on decadal variability, a 5 year running mean filter is applied to remove the field interannual variability. A narrower filter is not necessary, since, by construction, the POP technique is efficient in separating modes both in space and time.

The POP method reveals two stable modes of variability, each described by a pair of SST patterns. Each pattern corresponds to a phase in the temporal evolution. The first mode (Figure 1) explains 22% of the total variance and has a period of 13 years and an e-folding time of 45 years. The real POP (Figure 1(a)) is similar to the North Atlantic mode identified by Deser and Blackmon (1993). The real and the imaginary (with opposite signs) POPs together (Figure 1(a) and (b)) show how the positive SST anomalies originating in the Gulf Stream region are advected by the oceanic surface currents eastward, and afterwards southward

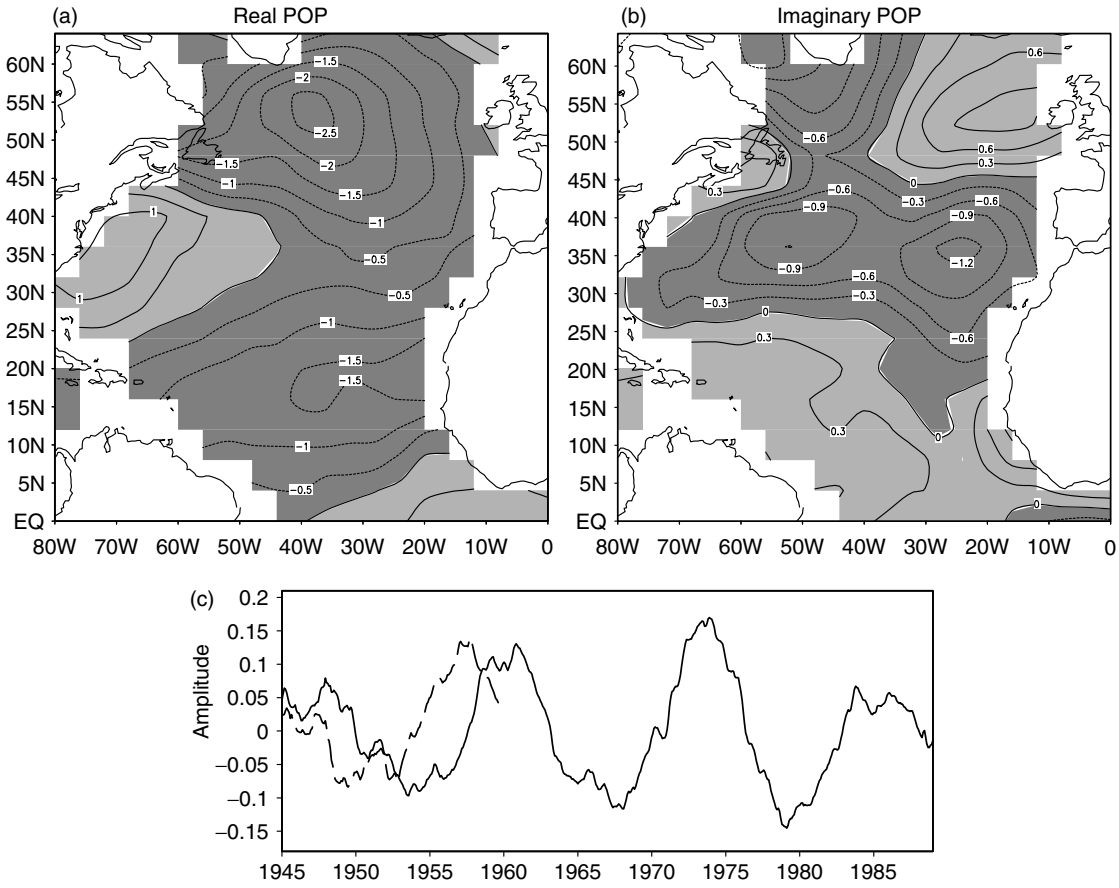

Figure 1. POP analysis of the anomalous COADS SST fields (degrees). (a) Real and (b) imaginary parts of the dominant POP (22%) obtained by analysing SST anomalies over the North Atlantic region, and (c) the corresponding real (solid line) and imaginary (dashed line) time components. The POP has a 13 year period and an e-folding time of 45 years

and northward respectively. The imaginary and real POP time-components (Figure 1(c)) are in quadrature, indicating a standing oscillation. The very long e-folding time of 45 years (more than three times longer than the period) and the other characteristics mentioned emphasize the high stability and prominence of this mode.

The second POP obtained (Figure 2) explains 8% of the variance in the field and has a 10 year period with an e-folding time of 18 years. The most representative feature of the imaginary part is the centre of positive values (Figure 2(b)) centred at [45 °N, 35 °W] and surrounded by anomalies of opposite sign. A similar centre located in the North Atlantic was derived based on solar irradiance for both decadal and multidecadal time scales (Lohmann *et al*., 2004: figure 2(a) and (c)). An almost identical centre associated with a long-term solar forcing was presented in Shindell *et al*. (2001: figure 1). In White *et al*. (1997: figure 6, top) the respective centre extends more eastward and has less of a latitudinal extension. The positive centre in (Figure 2(a)) is shifted northward in the real part of POP2, relative to the imaginary part (Figure 2(b)). The real structure follows the imaginary one after about quarter of the period (several years), consistent with a northward propagation of the SST anomalies along with the ocean surface currents (Sutton and Allen, 1997). The time components of the second POP are also in quadrature and describe a standing oscillation (Figure 2(c)). Overall, this POP is associated with a stable mode of climate variability. It is particularly important to note that POP2, although explaining a relatively small percentage of the variance, appears as a stable mode. This is consistent with the hypothesis that it is related to weak but steady forcing. The correlation coefficient between the imaginary time component and the sunspot cycle time series is −0.73 (Figure 2(c) and (d)).

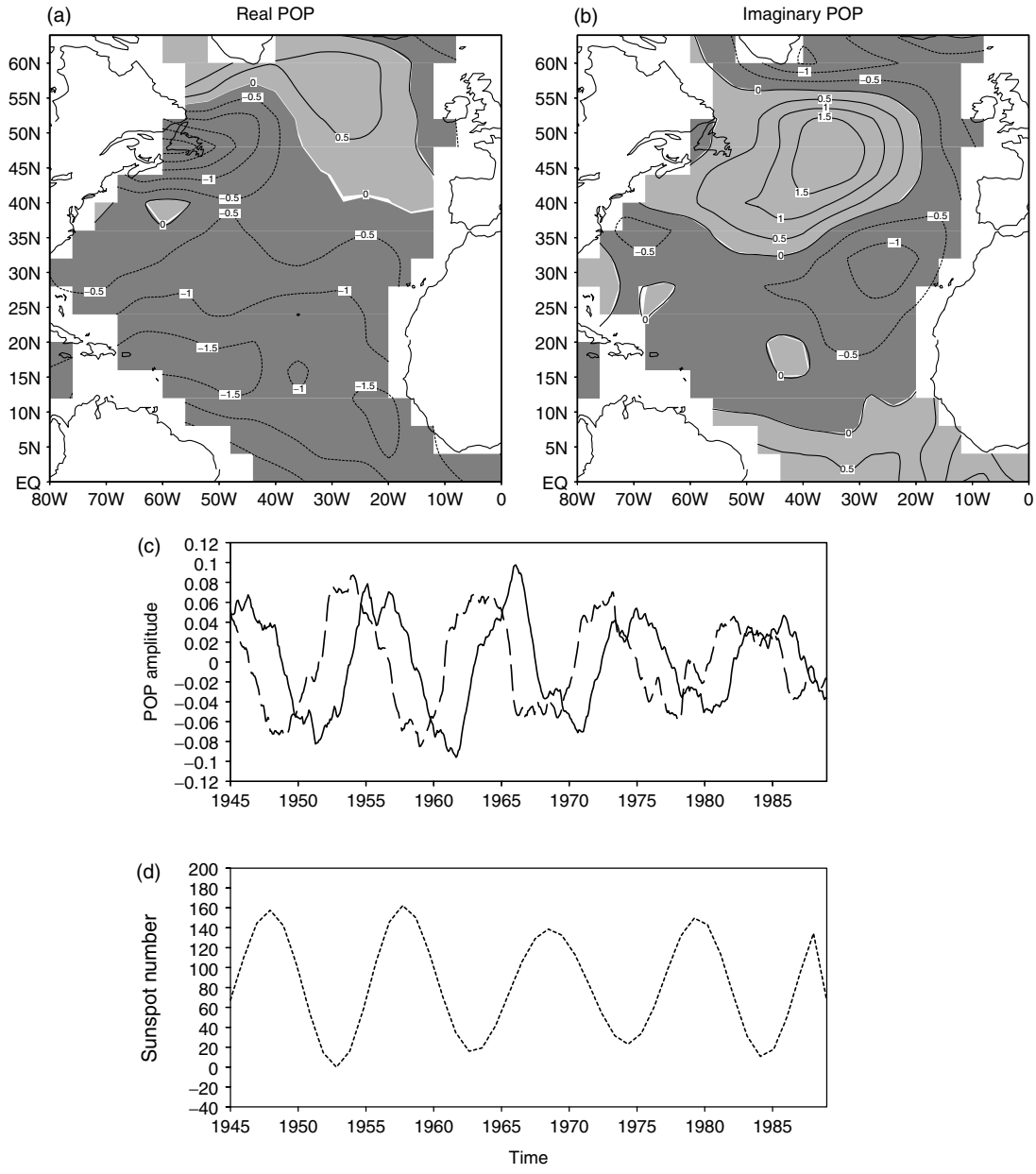

Figure 2. As Fig. 1, but for the second energetic POP (8%), which has a 10 year period and an e-folding time of 18 years. (d) The sunspot number time series filtered in the 9–14 year band

To summarize, the SST POP analysis reveals two stable and distinct decadal modes of climate variability, i.e. 13 and 10 years. The first mode can be identified with the mode described by Deser and Blackmon (1993) and is related to ocean–atmosphere interactions (Dima *et al*., 2001); the second mode has a distinct spatial pattern and initial results indicate it may be associated with the 11 year solar cycle.

3.2. EOF analysis of the SST field

The robustness of the distinction between the two quasi-decadal modes of variability in our analysis identified above is tested using several different data sets and methods. In order to extend the period analysed,

we used the longer SST data set provided by Kaplan *et al*. (1998), covering the 1856–1991 period. In order to emphasize modes in the decadal band, the annual data are filtered in the 9–14 year band prior to performing an EOF analysis on the data. The linear trend was also subtracted at every grid point prior to the analysis.

The first and the third SST EOFs emerging from the analysis are presented in Figure 3. The leading EOF (Figure 3(a)) explains 48% of the variance in this band. It is evident that this EOF1 of the decadal SST field is related to the 12–14 year cycle that dominates the North Atlantic surface climate variability at decadal time scales (Deser and Blackmon, 1993). The third SST EOF (EOF3), explaining 14% of the variance in the decadal band, has a distinct structure from that of EOF1 (Figure 3(b)), including a region of pronounced

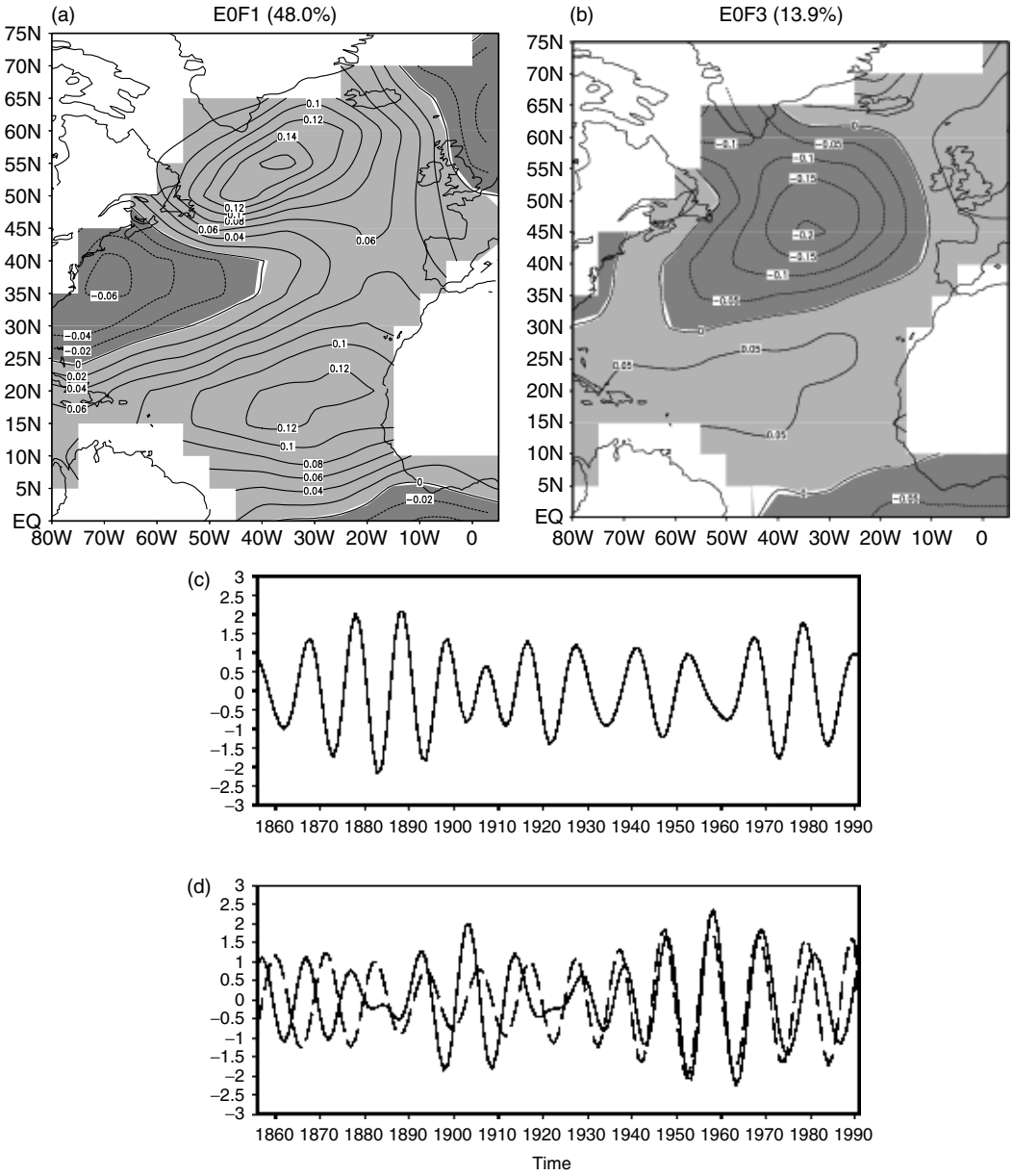

Figure 3. EOF analysis of the North Atlantic anomalous SST field (degrees) from Kaplan *et al*. (1998), filtered in the decadal frequency band. (a) First and (b) third EOFs and their PCs (c) and (d) obtained by analysing the Kaplan SST field covering the 1856–2000 period. The dotted line in (d) represents the sunspots number time series, filtered in the 9–14 years band

negative values centred at about 42 °N. The second EOF (not shown) is characterized by negative anomalies south of Greenland and positive values over almost all the rest of the basin and has a time component that is not significantly correlated at any lags with the principal components (PCs) PC1 or PC3. This spatially homogeneous pattern resembles very well the SST structure of the Atlantic multidecadal mode investigated in previous studies (Delworth and Mann, 2000). Since this mode is not of interest for the present study it will not be considered further.

The first and third PCs resulting from the filtered analysis are shown in Figure 3(c) and (d). No significant lag-correlation between PC1 and PC3 is obtained, consistent with the hypothesis that EOF1 and EOF3 do represent distinct modes of variability. An additional EOF analysis performed on the unfiltered SST data (not shown) reveals first (30.1%) and third (11.8%) EOFs that are practically identical to the corresponding modes identified using the filtered SST field.

PC3 and the sunspot number time series filtered in the 9–14 year band are shown in Figure 3(d). The correlation between the two time series is 0.47 for the whole period (1856–1991), and this increases to 0.65 when the more recent time period (1900–91) is considered (both correlations are significant at the 90% confidence level). These values further support the association between the two time components. On closer inspection one may notice that the two time series show in-phase variability during part of the last century, as well as some phase differences, mainly during the 19th century. If PC3 and SSC are connected, as we believe is the case, then the respective phase shifts may be explained if we consider that:

- PC3 is obtained by projecting EOF3 on the filtered SST data, a field where this mode explains a relatively small percentage of the variance (14%) and EOF1 is by far the dominant mode. Because the patterns of the two modes (EOF1 and EOF3) also include common characteristics (e.g. the region of positive values south of 25 °N), information related to the 12 year mode (EOF1/PC1) might be implicitly included in the third mode (EOF3/PC3), thus affecting the phase of the latter mode.
- The two decadal modes may also interact nonlinearly; therefore, linear methods like the EOF cannot derive the associated time components perfectly accurately.

These results do not rule out that PC3 and SSC might not be truly related as we assumed, and instead of EOF3 representing a mode of solar origins it might just represent another mode of internal origins, different from EOF1. Further analyses are performed in order to derive new constraints that support the solar origin hypothesis for EOF3.

The mode associated with the third SST EOF (Figure 3(b)) can also be obtained through EOF analyses performed on two different SST data sets in the North Atlantic sector: extended-COADS (Smith and Reynolds, 2003) and GISST (Parker *et al*., 1995) (not shown). In each of these analyses, the pattern associated with the third eigenvector (explaining 13% total variance for extended-COADS and 10% total variance for GISST) is close to identical to EOF3 in Figure 3.

Additional evidence for the link between the third surface mode described above (Figure 3(b)) and the sunspot solar cycle is given by the correlation map between the detrended decadal SSTs (Kaplan *et al*., 1998) and the solar cycle time component (Figure 4). The 11 year solar cycle was obtained by filtering the sunspot number time series in the 9–14 year band. The correlation coefficients between the solar mode and the SST field (Figure 4) are as large as −0.6. But by computing correlations one is not able to separate influences from other SST modes, which may explain why the correlation values are not uniformly high and significant over the whole North Atlantic basin. However, the close resemblance between the structure of this correlation map and the structures of the second imaginary POP (Figure 2(b)) and EOF3 in the SST data (Figure 3(b)), together with the 10 year period of the second POP, all provide strong support for considering this mode to be of solar origins.

3.3. POP analysis of the SLP field

In order to investigate the dominant modes of atmospheric variability, a POP analysis is performed on the Northern Hemisphere winter (December–February (DJF)) SLP field (20–90 °N) for the 1950–97 period (Trenberth and Paolino, 1980). Prior to the analysis, anomalies with respect to climatological values are

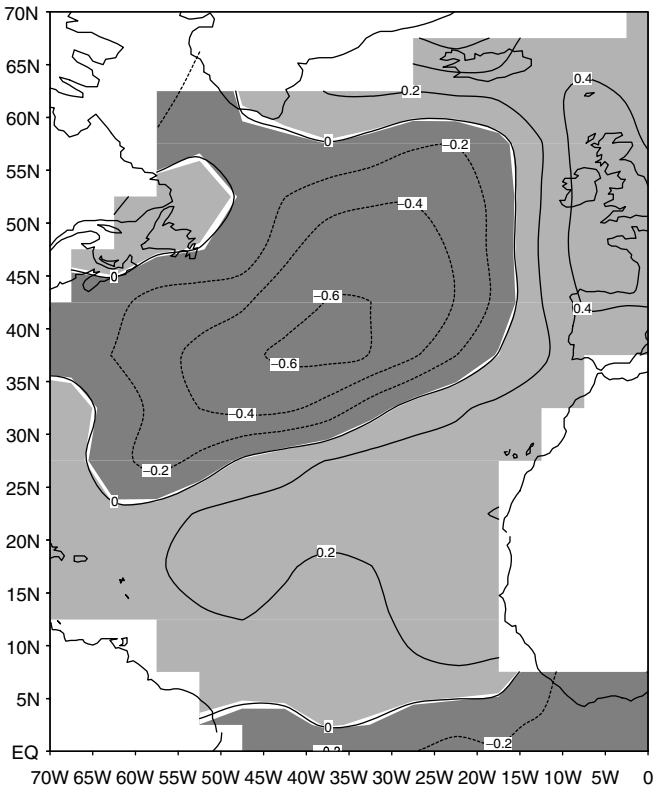

Figure 4. Correlation map between the 11 year solar cycle and the Kaplan SST field for the 1856–1991 period

computed, the linear trend at each grid point is subtracted, and a 5 year running-mean filter is applied in order to eliminate the interannual variability. The dominant SLP POP (Figure 5) has a period of 10.7 years and an e-folding time of 5.8 years. The imaginary and real time components (Figure 5(c)) are in quadrature with each other; thus, this mode has a high degree of stability. The correlation between the imaginary SLP POP time series and the solar cycle time component (filtered in the 9–14 year band) is highest (0.84) when the imaginary POP leads by 1 year. The imaginary part (Figure 5(b)) shows zonal symmetry with centres of positive anomalies located in the North Atlantic, North Pacific and over eastern Asia. Labitzke (2001: figure 1) also presented a zonally symmetric structure associated with the SSC, through a correlation map between the 11 year solar cycle and 30 hPa geopotential height. This common zonal symmetry feature indicates a very likely association between the SLP POP mode and the SSC, in which the stratosphere provides the physical link, as will be discussed in the next sections. It is interesting to note that the pattern in the North Pacific is changing from one phase (Figure 5(b)) to the other (Figure 5(a)), but the dipolar structure in the North Atlantic sector remains a stable feature.

The results presented so far support a persuasive distinction between the two decadal modes that emerged from our analyses. Whereas the first mode is identified as of internal origins, the second mode, which dominates the hemispheric SLP field, appears to be of solar origins. If this supposition were valid, then one would expect the solar mode to become more prominent in the upper atmospheric levels. This aspect is investigated in the next section.

4. MODES IDENTIFIED IN THE UPPER TROPOSPHERE

In order to investigate a potential solar signature at upper atmospheric levels, EOF analyses are performed on the 200 hPa streamfunction anomaly field, in the decadal band (9–14 years), using reanalysis data (Kalnay

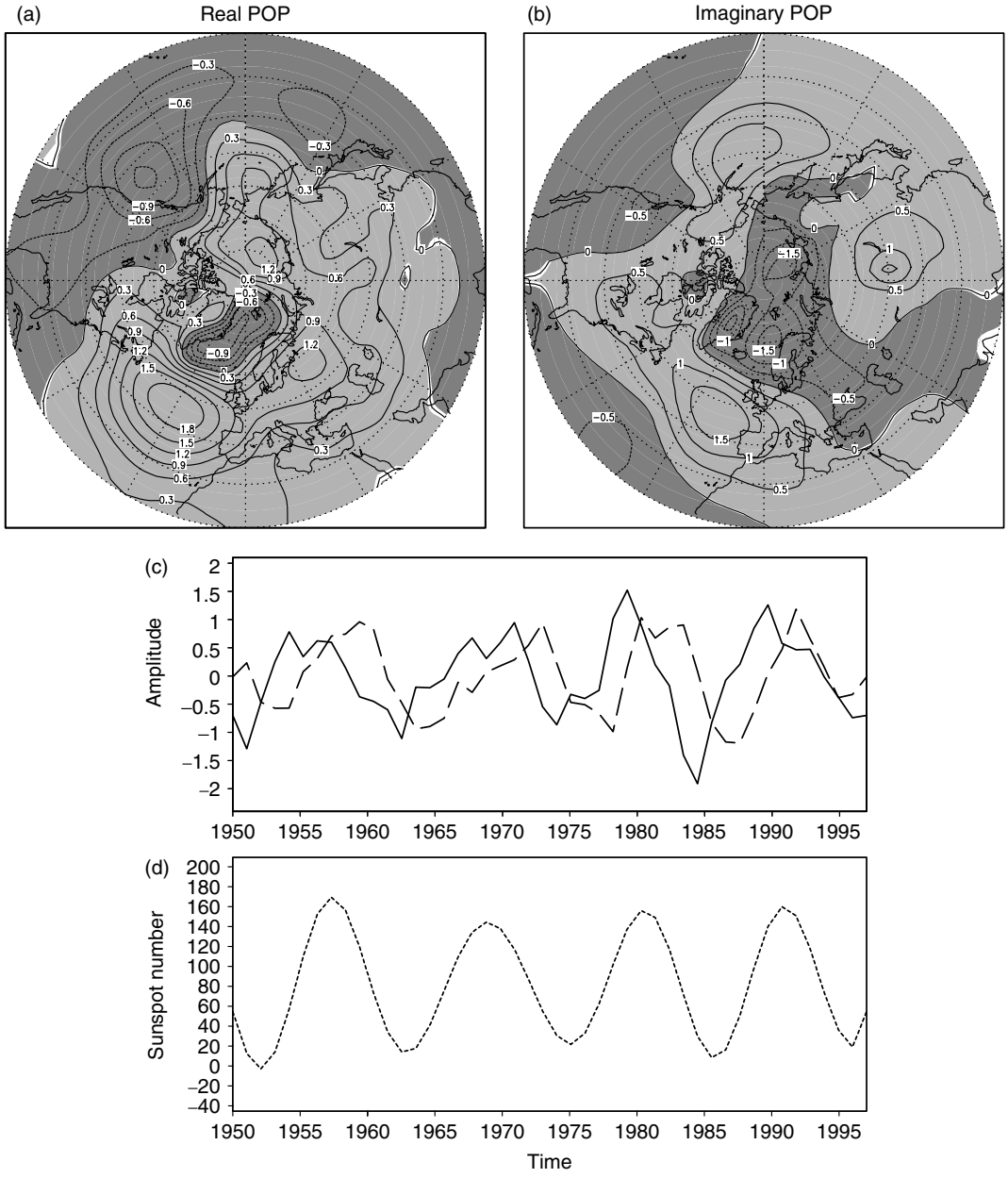

Figure 5. POP analysis of the anomalous SLP (hPa) data set of Trenberth and Paolino extending over the 1950–1997 period. (a) Real and (b) imaginary parts of the dominant POP obtained by analysing the SLP over the Northern Hemisphere, and the corresponding imaginary (solid line) and real (dashed line) components. The solid line is associated with the imaginary POP, and the dashed line corresponds to the real POP. The dotted line in (d) represents the sunspots number time series, filtered in the 9–14 years band

et al., 1996) covering the 1948–98 period. The first EOF analysis (Figure 6) was performed on the zonally averaged field (the case of EOF1), and a second EOF analysis (Figure 7) was performed on the same field but without zonal averaging beforehand (the case of EOF2). The reasons for these two different approaches are that one expects the zonal average of the streamfunction field to emphasize modes with zonal symmetry (as with solar mode forcing), whereas the zonal average diminishes the influence of the more regional modes (as is the case of the 12 year mode in the North Atlantic). Figures 6(a) and 7(a) show the PCs of EOF1

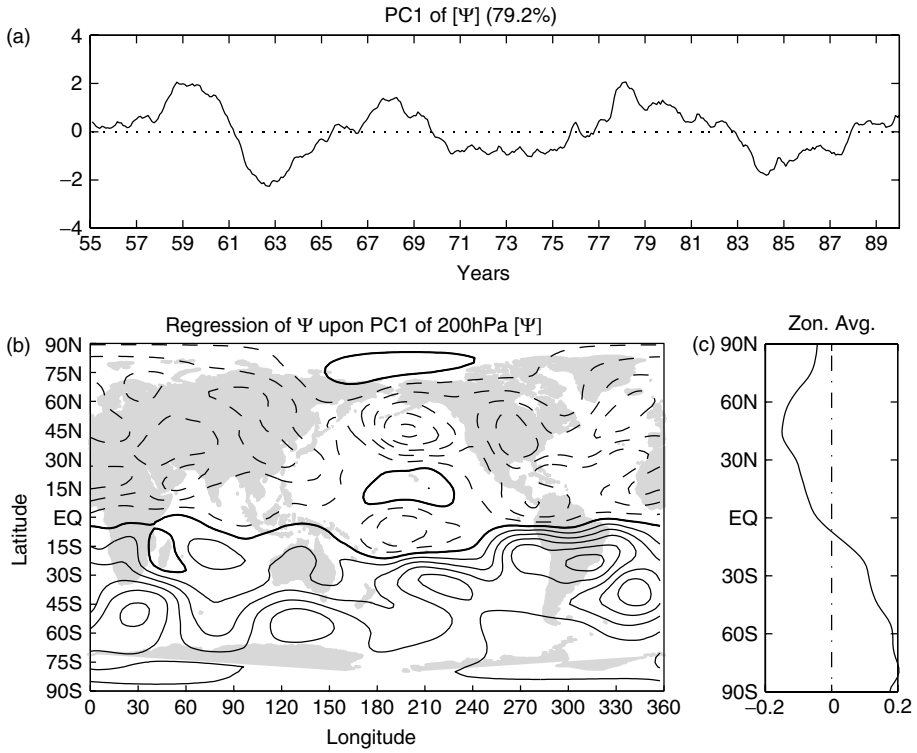

Figure 6. EOF analysis of the monthly 200 hPa streamfunction field. The PC time series (PC1) is shown in (a). Regression of monthly 200 hPa streamfunction upon PC1 of the 200 hPa 9–14 years filtered zonally averaged (b) and not zonally averaged (c) streamfunction field. Contour interval is 0.05 and represents degrees corresponding to a standard deviation of the PC1. The narrow panels on the bottom right shows the zonal average of the left-hand maps. The standardized PC1 time series is shown in (a). The streamfunction field represents anomalies with respect to the 1949–98 climatology

and EOF2 respectively, and Figures 6(b) and 7(b) display the regression coefficients of the monthly 200 hPa streamfunction upon their PCs. The corresponding EOFs (not shown) have very similar spatial structures to the regression maps shown in Figures 6(b) and 7(b) and explain 79.2% and 15.4% of the total variance in their bands respectively. The first mode is mainly characterized by negative streamfunction values in the Northern Hemisphere and positive values in the Southern Hemisphere (Figure 6(b) and (c)). The second mode (Figure 7(b)) consists of zonal bands of alternating signs and points to Hadley cell-related variability (Figure 7(c)), consistent with the mechanism proposed for the Atlantic quasi-decadal mode in the Northern Hemisphere (Dima *et al.*, 2001).

In order to test possible connections between these upper tropospheric modes and those identified at the surface, the unfiltered detrended SST field is regressed on the streamfunction time components shown in Figures 6(a) and 7(a). The SST field associated with PC1 of the zonally averaged streamfunction is displayed in Figure 8(a). It includes a centre of negative values in the central North Atlantic and anomalies of opposite sign around it. Although the extension of the centre is smaller, one can recognize the overall structure of the pattern to be similar to that of EOF3 of SST (Figure 3(b)), the imaginary part of the second POP of the North Atlantic SSTs (Figure 3(b)), and the correlation map of the SST field and the sunspot number time series (Figure 4), which suggests a common physical mechanism behind this upper tropospheric mode. The resemblance, although not perfect, is remarkable if one considers the small amount of variance explained by this mode in the decadal SST field (14%).

Furthermore, the SST pattern associated with PC2 of the streamfunction (Figure 8(b)) is much the same as the identified EOF1 of SST (Figure 3(a)) or the real part of the first POP of the North Atlantic region (Figure 1(a)). Note that the SST regression pattern of the streamfunction PC1 (Figure 8(a)) emphasizes a

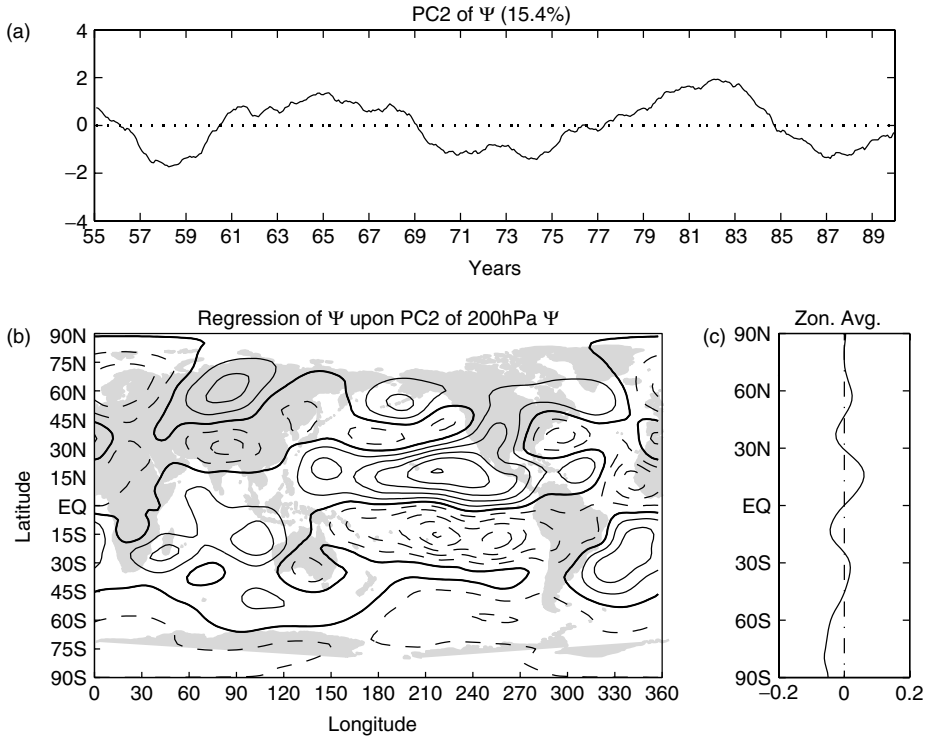

Figure 7. As Fig. 6, but for PC2. In this case, the EOF analysis is not performed on zonally averaged fields

structure that explains only 14% of variance in the decadal band. Therefore, the two streamfunction EOFs identified in the upper troposphere are linked to the modes identified in the surface temperature fields, but they emerge in reversed order from the analysis, which is consistent with the hypothesized different physical mechanisms behind these modes: the solar mode is dominant at higher levels in the atmosphere and in the SLP, whereas the internal mode, determined by ocean–atmosphere interactions, is dominant in the SST field.

By the same arguments, modes of a solar origin would be expected to explain a larger amount of variance at higher atmospheric levels, whereas modes resulting from air–sea interactions would be expected to be most influential in the lower atmosphere. The obvious dominance of the upper tropospheric leading mode (explaining 79.2% of the variance) and its association with the EOF3 in the SST field (explaining only 13.9% of variance in the decadal band) is, again, consistent with a solar origin of this mode. The relative importance of this mode compared with that of the internal mode decreases as the signal propagates from the stratosphere toward the surface. In an analogous manner, the second dominant mode in the upper troposphere (explaining only 15.4% of the variance at that level) is associated with the dominant surface mode of SST variability (where the mode explains 48% of SST variance in the decadal band). Thus, the relative importance of this decadal mode decreases as the signal propagates upward. These are all consistent with an internal origin for this mode based on atmosphere–ocean interactions.

In a recent study concerning the first two dominant coupled tropospheric–stratospheric modes (Itoh and Harada, 2004) it is shown that the Northern Hemisphere atmospheric zonally symmetric mode (the annular mode) propagates downward from the stratosphere towards the troposphere, while the zonally asymmetric mode (associated with the Pacific–North American (PNA) structure) propagates upward, from the troposphere into the stratosphere, in about a week. In the context of our study, the SSC mode, through the imaginary POP of the SLP field, projects strongly onto the annular mode, while the atmospheric part of the Atlantic quasi-decadal mode projects onto the PNA mode (Dima *et al*., 2002).

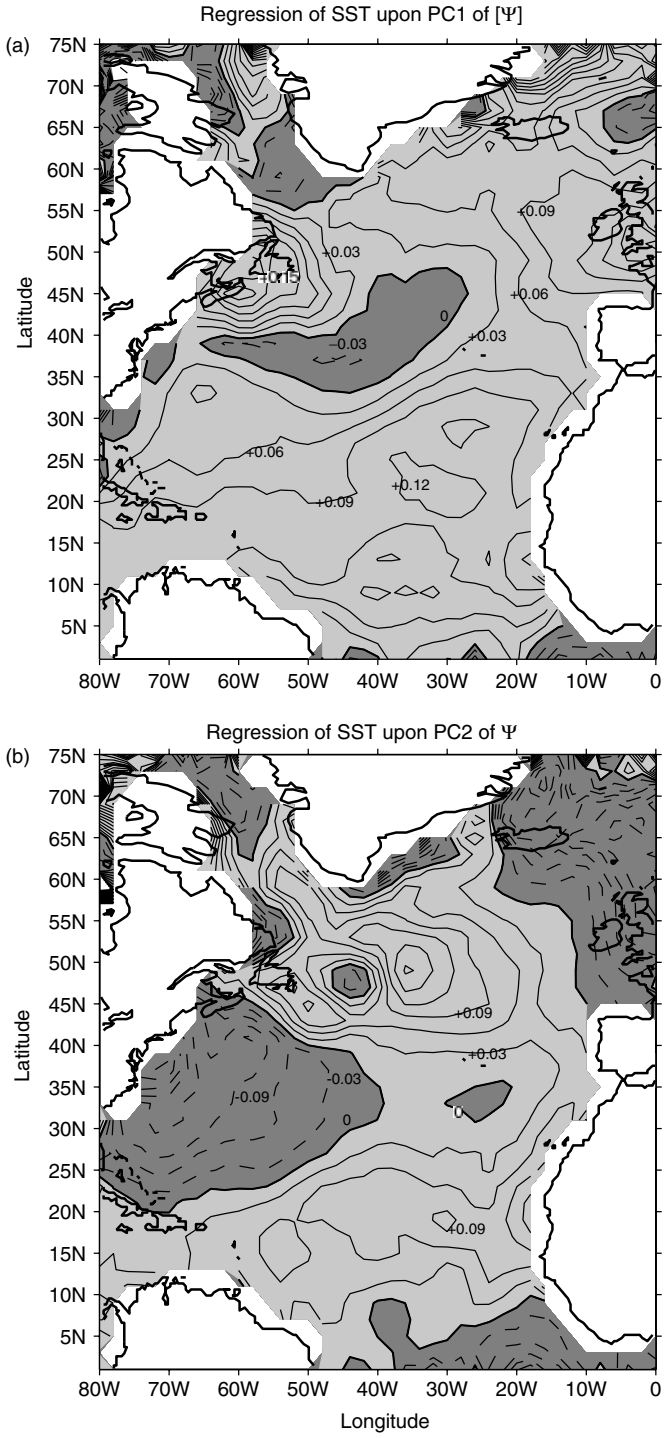

Figure 8. Regression of the anomalous detrended SST field (degrees) for the 1948–97 period, upon (a) PC1 and (b) PC2 of the 200 hPa 9–14 years filtered streamfunction fields in Figures 6(a) and 7(a) respectively

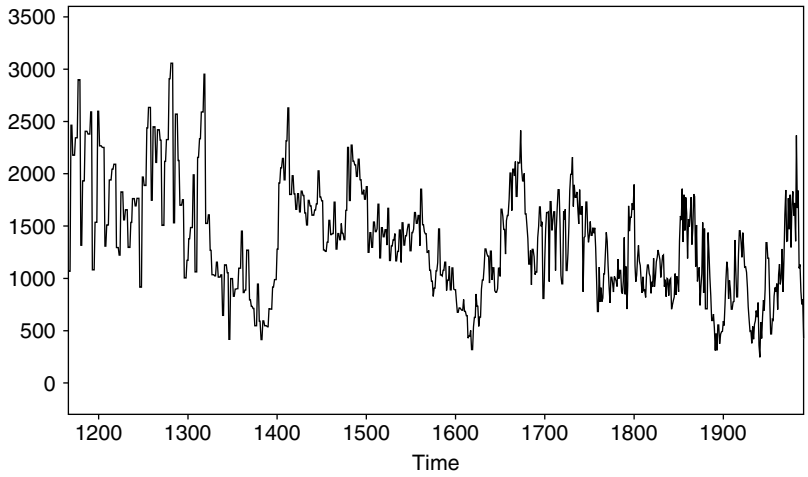

Figure 9. Sediment-based reconstructed time series from the Cariaco basin (Black *et al*., 1999)

5. IDENTIFICATION OF DECADAL MODES IN RECONSTRUCTED TIME SERIES

By applying EOF and POP methods in the space–time domain, on different sets of data, the distinction between two quasi-periodic decadal modes has been emphasized. These analyses are now extended by applying a different method, i.e. SSA (Allen and Smith, 1997), in the time domain. A long proxy record with relatively high resolution is used to identify the decadal modes. Sediment records from the Cariaco basin in the southern Caribbean provide a millennial proxy for ocean–atmosphere variability in the North Atlantic basin (Black *et al*., 1999), reflecting variations in the strength of the trade winds, the position of the intertropical convergence zone and the amplitude of SST. This record covers the 1166–1990 time period and it is interpolated to an annual resolution (Figure 9).

A preliminary SSA analysis using a 300 year window shows that the Cariaco time series includes a rich spectrum of quasi-periodic components. To focus on the decadal time scale components, the time series is reconstructed based on its first 12 components with periods longer than 50 years. This reconstructed component is then subtracted from the initial time series to obtain a residual record, which would then contain time scales smaller than 50 years. A similar procedure was used by Chao *et al*. (2000). In order to identify decadal modes of variability a 50 year window is then used in a new SSA applied to the residual time series obtained. Among other periodic components, this technique identifies two quasi-decadal periodic signals (Figure 10(b) and (d)) for the 1856–1990 time period. The time EOFs associated with the first decadal component (Figure 10(a)) are in quadrature with each other and their corresponding eigenvalues are close to each other in the eigenvalues spectrum, thus indicating a stable oscillation. The reconstructed time component (Figure 10(b)) oscillates regularly with an $\sim$13 year period and explains 15% of the total variance. The second component (Figure 10(d)) represents a standing oscillation as well, as suggested by its associated time EOFs (Figure 10(c)). It has a period of $\sim$10 years and explains 4% of the total variance. It is important to note that the two decadal time components identified through the SSA have periods identical to those of the modes identified in the SST field through the POP method, although the time series analysed here covers a much longer time period. Moreover, as in the POP and EOF analyses of the SST, the 13 year mode explains approximately three times more variance than the 10 year mode. This quantitative assessment of the relative roles played by these two modes is thus estimated based not just on the instrumental period, but also on a long proxy record. This suggests that the information inferred from the observational data is also suggestive for much longer time intervals, extended back in time.

The SST field provided by Kaplan *et al*. (1998) is regressed on both time series identified by the SSA. The resulting patterns are shown in Figure 11. The SST pattern associated with the $\sim$13 year period time component (Figure 11(a)) is very similar to EOF1 of SST (Figure 3(a)). Furthermore, the pattern

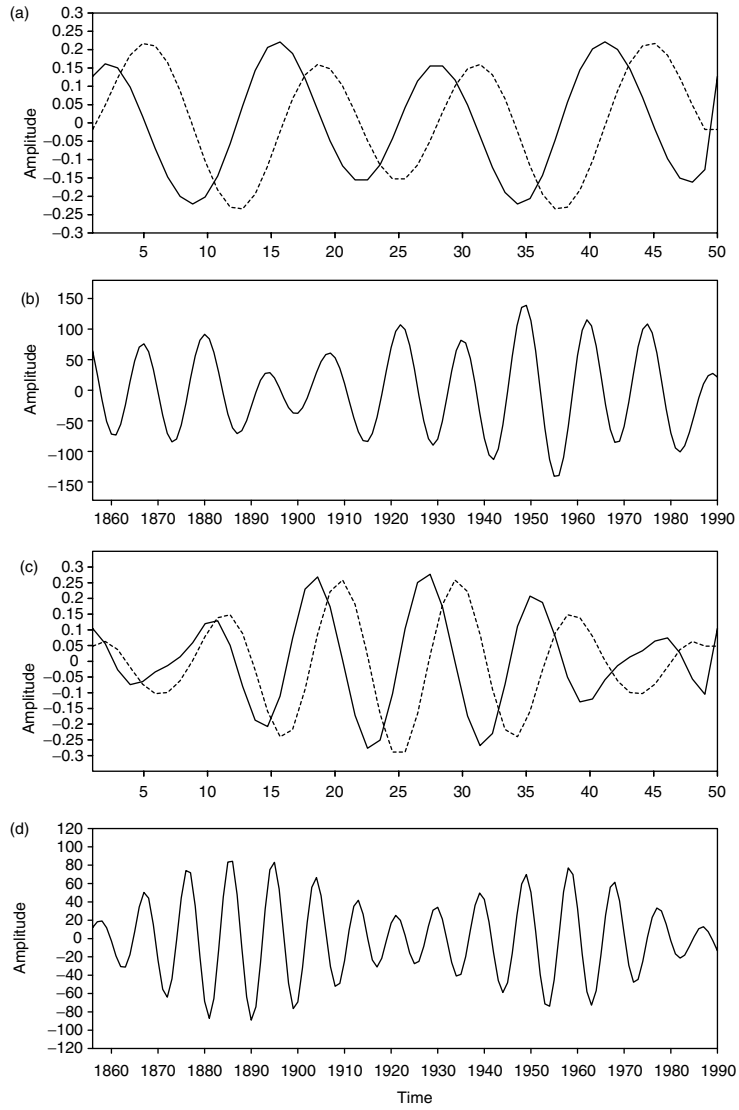

Figure 10. SSA of the Cariaco reconstruction. (a) Time EOFs associated with the ∼13 year period time-component, which is shown in (b). (c) Time EOFs associated with the ∼10 year period time-component, which is shown in (d)

associated with the ∼10 year period time component (Figure 11(a)) is close to identical to the EOF3 of SST (Figure 3(b)) or the correlation map shown in Figure 4. One may note that this last pattern is revealed through correlations, although it explains only a small amount of the variance in the decadal band of the SST field (14%).

Therefore, the SSA analysis of the sediment-based reconstructed component proves efficient in making a distinction in the time domain between two modes of decadal time scales. This was also possible because of the relatively long period, the high temporal resolution and the good quality of this proxy record. One notes that the two modes identified here are consistent with 12–13 year mode reported by Black *et al*. (1999) in their sediment-based reconstruction and with the solar signature in the SST field, including a centre of anomalies in the central North Atlantic that is visible in their analysis (figure 1 in their study), a pattern which we associated with the solar cycle. The separation identified in the time domain further supports the distinction between the two quasi-decadal modes, as it was also emphasized using other data and methods.

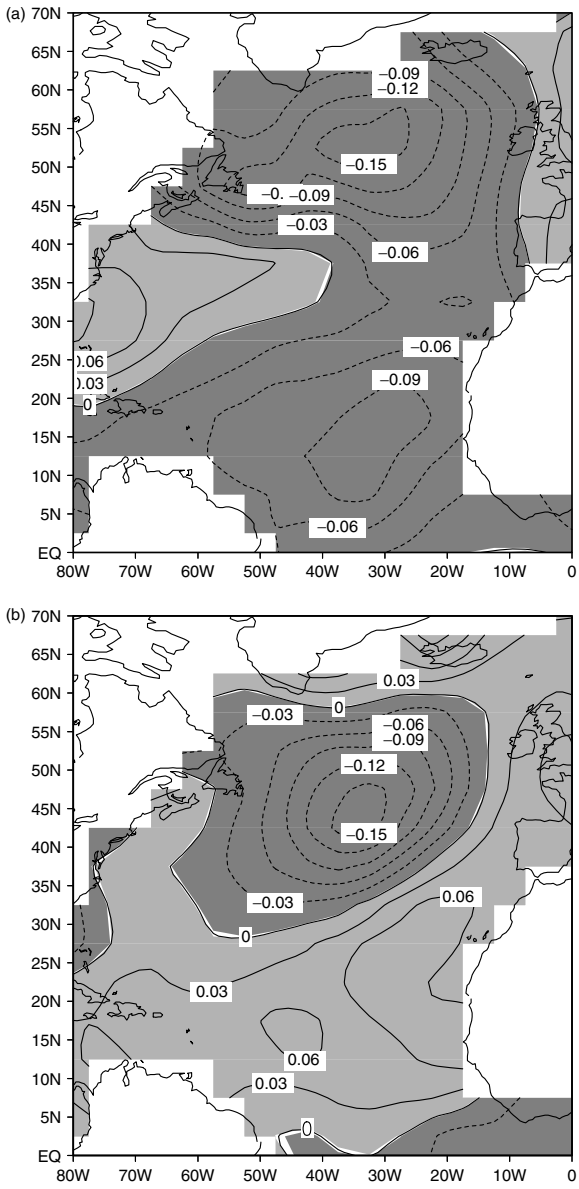

Figure 11. Regression maps of the Kaplan SST field on the decadal time components identified through SSA for the Cariaco time series. (a) The ∼13 year time component; (b) the ∼10 year time component

6. DISCUSSION

Several statistical analyses applied on different sets of data emphasize a clear distinction between a mode linked to internal variability and another mode connected to solar forcing. A synthesis of the results is presented in Table III.

The POP method performs a simultaneous space–time separation and, as a result, it provides essential information about each climatic mode that it emphasizes the method gives two patterns that describe the dynamical spatial evolution of the mode, as well as its corresponding period and damping time. The analysis identifies two distinct modes of variability with periods of 13 years and 10 years (Figures 1 and 2 respectively).

Table III. Synthesis of the results

Method	Field	Figure	Results
POP	SST	1, 2	Shows a distinction between two modes with different spatial patterns and periods of 13 and 10 years
EOF	SST	3	Emphasizes the distinct patterns of the decadal modes; the patterns are almost identical with those obtained from the POP analysis
Correlation	Sunspots number–SST	4	The correlation map is very similar to the patterns of the 10 year period POP and that of the SST EOF3
POP	SLP	5	Emphasizes a POP with a 10.7 year period; the imaginary POP is almost identical to the leading mode of the height field at 500 hPa (Baldwin *et al*., 1994) and to the 30 hPa geopotential height correlation map presented by Labitzke (2001)
EOF	Streamfunction	6, 7	Shows two distinct modes of variability; the leading two EOFs explain 79.2% and 15.4% of the total variance
Regression	SST–streamfunction PCs	8	Emphasizes SST structures that are very similar to the modes identified by POP and EOF analyses of the SST fields
SSA	Proxy record	9, 10	Emphasizes two decadal time components with periods of 13 and 10 years
Regression	SST–SSA components	11	Shows that the SST patterns associated with the SSA decadal time components are almost identical to the structures identified by POP and EOF analyses of the SST fields

The first mode identified has a tripolar structure, as the pattern described by Deser and Blackmon (1993), and the second mode is characterized by a region of negative anomalies centred at 45 °N, 35 °W, similar to the pattern identified in association with multidecadal fluctuations of the solar forcing (Shindell *et al*., 2001). We note that Lohmann *et al*. (2004) associated the same SST structure with both the decadal and the multidecadal solar forcing.

The distinction between these two decadal modes is confirmed by EOF analyses on different annual SST fields. The first and the third SST EOFs emerging from these analyses are close to identical to the two modes identified through the SST POP analysis. SST PC3 shows in-phase variability with the sunspot cycle during part of the last century, as well as some phase differences mainly during the 19th century. The phase shifts could have at least two different causes:

- The PC3 is obtained by projecting EOF3 on the initially filtered SST field, in which this mode explained a relatively small percentage of the variance and PC1 is dominant. Because the patterns of the two modes include some common features, the information related to the 12 year mode may affect the phase of the PC3.
- The two decadal modes may interact nonlinearly and, therefore, it is not possible to derive their time components accurately using linear methods.

Further analysis supports the solar origin of the SST EOF3. The structure of the correlation map between the decadal SST and the solar cycle time component is very similar to that of the SST EOF3 and the imaginary part of the second mode obtained through the POP analysis. The structure of these modes, including distinct anomalies in the central North Atlantic, is similar to that presented by Shindell *et al*. (2001) in association with the solar forcing, based on model integrations.

The POP analysis performed on the Northern Hemisphere winter SLP field (20–90 °N) for the 1950–97 time period (Trenberth and Paolino, 1980) emphasizes a dominant mode with a period of 10.7 years and an e-folding time of 5.8 years, connected with the sunspots time series. The SLP POP provides the key link between the solar forcing and its fingerprint in the SST field (Figures 3(b) and (4)). The POP imaginary part (Figure 5(b)) shows a strong zonal symmetry with centres of positive anomalies located in the North Atlantic, North Pacific and over eastern Asia. The structure of the imaginary SLP POP is close to identical to the DJF 500 hPa height map presented by Baldwin *et al.* (1994). The pattern in their study (emerging as a leading mode) was derived through a singular value decomposition analysis between the DJF 500 and 50 hPa height fields (figure 3 in their study). This very close resemblance between a zonally symmetric mode identified in the SLP field and a 500 hPa height structure strongly coupled to the height field at 50 hPa clearly suggests that the SLP structure is induced from the stratosphere. This is consistent with the observation that the dominant mode in the SLP field may be interpreted as the surface modulation in the strength of the polar vortex (Thompson and Wallace, 1998). This is also supported by Black (2002), who showed that the AO-related surface climate variations are strongly linked to the strength of the stratospheric polar vortex. These surface climate variations are due to large-scale potential vorticity anomalies in the lower stratosphere, associated with changes in the strength of the stratospheric polar vortex that induces zonally symmetric zonal wind perturbations extending downward to the surface. This is characterized as a large-scale annular stirring of the troposphere from above (Black, 2002) and is consistent with the fingerprint of the 11 year solar cycle identified in the lower atmosphere by Coughlin and Tung (2004).

Our results are also supported by the study of Labitzke (2001). For example, the structure of the imaginary SLP POP (Figure 5(b)) is very similar to the correlation map between the 11 year solar cycle and 30 hPa geopotential height presented by Labitzke (2001). A dynamical link between solar irradiance and the stratospheric polar vortex has been attributed to an interaction between ultraviolet radiation and ozone in the stratosphere (Balachandran *et al.*, 1999) and a downward propagation of stratospheric events (Baldwin and Dunkerton, 1999; Christiansen, 2000). The new information provided by the SLP POP analysis is the period of the dominant mode in this field. Therefore, aside from the similarity with leading upper atmosphere modes, the dominant POP has an ~10 year period, consistent with a sunspot cycle origin. Furthermore, together the almost identical structure of the real SLP POP, the 500 hPa mode presented by Baldwin *et al.* (1994) and the 30 hPa correlation map (Labitzke, 2001), in association with the identified 10 year period of the SLP POP, provide strong support for a fingerprint of the solar mode in the troposphere.

In order to complete the analysis of the solar forcing mechanism down to the ocean, it is worth analysing the relation between the SLP POP and the ocean surface conditions. The structure of the SLP POP in the North Atlantic sector is qualitatively the same in the imaginary (Figure 5(b)) and the real POPs (Figure 5(a)). The bipolar structure resembles the NAO. It is important to observe that the position of the dipole zonal axis (the imaginary line perpendicular to the maximum SLP gradient) is shifted northward relative to that corresponding to the NAO-like structure associated with the SST tripole, which is disposed at approximately 50 °N (Dima *et al.*, 2001). A similar northward shift of the centre of positive SST anomalies extending eastward from North America is observed in Figures 1(a) and 2(b), in association with the 13 year and 10 year modes. In the case of the tripolar SST mode, the associated NAO-like structure appears to induce SST anomalies that expand eastward from the Gulf Stream region through the associated wind conditions (Figure 1(a)), in a similar way to that described by Dima *et al.* (2001). In a similar manner, the shifted NAO structure associated with the solar forcing (Figure 5(a)) may determine the amplitude of the SST anomalies centred at 47 °N (Figure 2(b)). In other words, in the solar mode case (Figure 5(a) and (b)), since the zonal axis of the SLP dipole is being shifted northward, the SST fingerprint is consequently shifted northward as well, from the position noted in the 13 year mode case.

Our results are consistent with the model integration of Shindell *et al.* (2001), which emphasizes a surface temperature pattern in the North Atlantic sector that is close to identical to that in Figure 2(b). Note that in their experiment the ocean included only a mixed layer; therefore, ocean dynamics are not responsible for generating that particular structure. Furthermore, the EOF analysis of the streamfunction fields at 200 hPa emphasizes a dominant mode with pronounced zonal symmetry (Figure 6) consistent with that mode being

of solar origin. Regression of this mode onto the SST field gives a pattern similar to EOF3 of the SST field (Figure 3(b)).

An SSA performed on a time series reconstructed from sediment records in the Cariaco basin (Black *et al*., 1999) covering the 1166–1990 period emphasizes two modes with decadal time scales. When regressed onto the SST fields, these time components generate two distinct structures very similar to the corresponding modes derived from the POP and EOF analyses of the SST fields. It is worth noting that in three analyses (POP and EOF analyses of the SST and SSA on the Cariaco proxy record), the 13 year mode explains approximately three times more variance than the 10 year mode, thus providing a mutually consistent quantitative assessment of the relative roles played by these two modes in the oceanic surface layers.

Overall, the solar mode appears as having a relatively weak, but still stable, fingerprint in the SST field, which is consistent with a weak but steady solar forcing. The fact that a mode explaining moderate percentages of the variance in the SST field is consistently recovered in different analyses and data sets may be explained by the integrating effect of the ocean on the solar component while filtering the atmospheric noise.

To summarize, the robustness of the distinction between the two decadal modes of variability identified is supported by the following considerations:

1. Different statistical techniques are used: POP (space–time domain), EOF (space domain), and SSA (time domain).
2. Different data sets (not all of them are totally independent) are considered for the calculations: SST (da Silva *et al*., 1989; Parker *et al*., 1995; Kaplan *et al*., 1998; Smith and Reynolds, 2003), streamfunction (Kalnay *et al*., 1996; Kistler *et al*., 2001) and a sediment-based reconstruction from the Cariaco basin (Black *et al*., 1999).

The solar origin of the mode associated with EOF3 (Figure 3(b)) derived from the SST data (Kaplan *et al*., 1998) is supported by several results:

1. The structure of the correlation map between the sunspots number time series and the SST field (Figure 4) is almost identical to that of the SST EOF3.
2. The associated time component (PC3) is significantly correlated to the sunspots number time series.
3. The second POP of the COADS SST data has the same structure as the correlation map and as the SST EOF3 map, and its period is 10 years, very close to the recurrence interval of the sunspot numbers.
4. The SST EOF3 (Figure 3(b)) is not the dominant mode of variability at the surface, but it becomes the leading mode of variability at the 200 hPa level (Figures 6 and 8(a)); therefore, the amplitude of the signature of this mode decreases as the signal propagates toward the surface.
5. The results presented here, corroborated by previous studies (Baldwin *et al*., 1994; Labitzke, 2001), are consistent with the mechanism through which the solar influence is transmitted from the stratosphere to the surface (Black, 2002).

7. CONCLUDING REMARKS

Our analysis shows two distinct modes of climate variability at a decadal time scale. Statistical methods applied to instrumental, reanalysis and proxy data emphasize the North Atlantic fingerprint of a quasi-decadal mode (Deser and Blackmon, 1993), which has been connected to atmosphere–ocean interactions (Dima *et al*., 2001). Furthermore, a pattern that explains less variance in the SST is obtained that is very similar to what is found in numerical experiments in association with solar forcing (Shindell *et al*., 1999, 2001) and in observational data (Lohmann *et al*., 2004) for decadal and multidecadal time scales associated with the Schwabe and Gleissberg solar irradiance cycles (Hoyt and Schatten, 1997). In the upper atmospheric levels and in the SLP, this mode dominates the climate variability at decadal time scales.

A dynamical link between the solar irradiance and the stratospheric polar vortex has been attributed to an interaction between ultraviolet radiation and the ozone in the stratosphere (Balachandran *et al*., 1999). The

present results are consistent with the view in which potential vorticity anomalies in the lower stratosphere, associated with changes in the strength of the stratospheric polar vortex, induce zonally symmetric zonal wind perturbations extending downward to the surface, like a large-scale annular stirring of the troposphere from above (Black, 2002). In turn, these atmospheric circulation anomalies affect the ocean surface conditions.

For a mechanistic understanding of the solar–climate link and the separation of internal and solar-induced variations, long-term measurements and modelling studies are required, especially in the upper atmosphere, where the solar influence on climate is strongest (Haigh, 1999; Shindell *et al*., 1999). Our approach uses several observational, reanalysis and proxy data sets and complementary statistical methods in order to reduce the uncertainty in the results. Consequently, if these distinct analyses based on different data sets provide convergent results which are consistent with our hypothesis and with previous studies, then this provides support for our assumption and suggests that the limitations of the data sets were successfully minimized.

The study shows that the internal mode and the cycle linked to the sunspot number variations are detected in the spatial domain of long-term instrumental and reanalysis data, as well as in the time domain through the time series analysis of a high-resolution sediment core from Cariaco basin. The heterogeneous set of data and methods emphasize the distinction between the two decadal modes and their associated different origins and quantifies their relative importance in the surface and upper atmospheric layers. At the surface, the mode linked to atmosphere–ocean interactions explains about three times more variance than the mode associated with the solar sunspots cycle. The solar mode dominates the variability at higher levels of the atmosphere, providing support for a mechanism through which the solar influence is transmitted downward from the stratosphere. Identifying these modes and being able to separate them is important for understanding the past and future, natural and forced climate variability.

ACKNOWLEDGEMENTS

We thank two anonymous reviewers for helpful comments and acknowledge the support of the Alexander von Humboldt Foundation, the German Federal Ministry for Education and Research through the DEKLIM project and the German Science Foundation DFG through the Research Centre of Ocean Margins. This article has AWI number 14 988. I. M. Dima was supported by the NSF grant ATM 0 318 675.

REFERENCES

Allen M, Smith LA. 1997. Optimal filtering in singular spectrum analysis. *Physics Letters* **234**: 419–428.

Balachandran NK, Rind D, Lonergan P, Shindell DT. 1999. Effects of solar cycle variability on the lower stratosphere and troposphere. *Journal of Geophysical Research* **104**: 27 321–27 339.

Baldwin MP, Dunkerton TJ. 1999. Downward propagation of the Arctic oscillation from the stratosphere to the troposphere. *Journal of Geophysical Research* **104**: 30 937–30 946.

Baldwin MP, Cheng X, Dunkerton TJ. 1994. Observed correlations between winter-mean tropospheric and stratospheric circulation anomalies. *Geophysical Research Letters* **12**: 1141–1144.

Black XR. 2002. Stratospheric forcing of surface climate in the Arctic oscillation. *Journal of Climate* **15**: 268–277.

Black DE, Peterson LC, Overpeck JT, Kaplan A, Evans MN, Kashgarian M. 1999. Eight centuries of North Atlantic ocean–atmosphere variability. *Science* **286**: 1709–1713.

Chao Y, Ghil M, McWilliams JC. 2000. Pacific interdecadal variability in this century's sea surface temperatures. *Geophysical Research Letters* **27**: 2261–2264.

Christiansen B. 2000. A model study of the dynamical connection between the Arctic oscillation and stratospheric vacillations. *Journal of Geophysical Research* **105**: 29 461–29 474.

Coughlin K, Tung KK. 2004. Eleven-year solar cycle signal throughout the lower atmosphere. *Journal of Geophysical Research* **109**: 1–17. DOI: 10.1029/2004JD004873.

Cubasch U, Voss R, Hegerl GC, Waszkewitz J, Crowley TJ. 1997. Simulation of the influence of solar radiation variations on the global climate with an ocean–atmosphere circulation model. *Climate Dynamics* **13**: 757–767.

Da Silva AM, Young AC, Levitus S. 1994. *Algorithms and Procedures. Vol. 1, Atlas of Surface Marine Data 1994*. National Oceanic and Atmospheric Administration.

Delworth TL, Mann ME. 2000. Observed and simulated multidecadal variability in the Northern Hemisphere. *Climate Dynamics* **16**: 661–676.

Deser C, Blackmon ML. 1993. Surface climate variations over the North Atlantic Ocean during winter: 1900–1989. *Journal of Climate* **6**: 1743–1753.

Dima M, Rimbu N, Stefan S, Dima I. 2001. Quasi-decadal variability in the Atlantic basin involving tropics–midlatitudes and ocean–atmosphere interactions. *Journal of Climate* **14**: 823–832.

Dima M, Rimbu N, Dima I. 2002. Arctic oscillation variability generated through inter-ocean interactions. *Geophysical Research Letters* **29**(14): 22:1–4. DOI: 10.1029/2002GL014717.

Grötzner AM, Latif M, Barnett TP. 1997. A decadal climate cycle in the North Atlantic Ocean as simulated by the ECHO coupled GCM. *Journal of Climate* **11**: 831–847.
Haigh JD. 1999. A GCM study of climate change in response to the 11-year solar cycle. *Quaterly Journal of the Royal Meteorological Society* **125**: 871–892.
Hansen JE, Lacis AA. 1990. Sun and dust versus green-house gases: an assessment of their relative roles in global climate change. *Nature* **346**: 713–719.
Hasselman K. 1988. PIPs and POPs: the reduction of complex dynamical systems using principal interaction and oscillation patterns. *Journal of Geophysical Research* **93**: 11 015–11 021.
Hoyt DV, Schatten KH. 1997. *The Role of the Sun in Climate Change*. Oxford University Press: New York.
Hurrel JW. 1995. Decadal trends in the North Atlantic oscillation: regional temperatures and precipitation. *Science* **269**: 676–679.
Itoh H, Harada K. 2004. Coupling between tropospheric and stratospheric leading modes. *Journal of Climate* **17**(2): 320–336.
Jones RH. 1975. Estimating the variance of time averages. *Journal of Applied Meteorology* **14**: 159–163.
Kalnay E, Kanamitsu M, Kistler R, Collins W, Deaven D, Ganolin L, Iredell M, Saha S, White G, Woollen J, Zhu Y, Leetmaa A, Reynolds B, Chelliah M, Ebisuzaki W, Higgins W, Janowiale J, Mo KC, Ropelewski C, Wang J, Jenne R, Joseph D. 1996. The NCEP/NCAR reanalysis project. *Bulletin of the American Meteorological Society* **77**: 437–471.
Kaplan A, Cane MA, Kushnir Y, Clement AC, Blumenthal MB, Rajagopalan B. 1998. Analyses of global sea surface temperature 1856–1991. *Journal of Geophysical Research* **103**: 27 835–27 860.
Kistler R, Kalnay E, Collins W, Saha S, White G, Woollen J, Chelliah M, Ebisuzaki W, Kanamitsu M, Kousky V, van den Dool H, Jenne R, Fionino M. 2001. The NCEP–NCAR 50-year reanalysis: monthly means CD-Rom and documentation. *Bulletin of the American Meteorological Society* **82**: 247–267.
Labitzke K. 2001. The global signal of the 11-year sunspot cycle in the stratosphere: differences between solar maxima and minima. *Meteorologische Zeitschrift* **10**: 83–90.
Lean J, Beer J, Bradley R. 1995. Reconstruction of solar irradiance since 1610: implications for climate change. *Geophysical Research Letters* **22**(23): 3195–3198.
Leith CE. 1973. The standard error of time-average estimates of climatic means. *Journal of Applied Meteorology* **12**: 1066–1069.
Lohmann G, Rimbu N, Dima M. 2004. Climate signature of solar irradiance variations: analysis of long-term instrumental, historical and proxy data. *International Journal of Climatology* **24**: 1045–1056.
McKinnon JA. 1987. Sunspot numbers 1610–1985. World Data Center A for Solar Terrestrial Physics, Boulder.
Mitchell JFB, Karoly DJ, Hegerl GC, Zwiers FW, Allen MR, Marengo J. 2001. Detection of climate change and attribution of causes. *In Climate Change 2001: The Scientific Basis*, Houghton JT, Ding Y, Griggs DJ, Noguer M, van der Linden PJ, Dai X, Maskell K, Johnson CA (eds). Cambridge University Press: Cambridge, UK/New York, USA.
Parker DE, Folland CK, Bevan A, Ward MN, Jackson M, Maskell F. 1996. Marine surface data for analysis of climate fluctuations on interannual to century time-scales. In *Natural Climate Variability on Decade-to-century-timescales*, National Research Council, Martinson DG, Bryan K, Ghill M, Hall MM, Karl TR, Sarachik ES, Sorooshian S, Talley LD (eds). National Academy Press: Washington DC; 241–250.
Rind D. 2002. The sun's role in climate variations. *Science* **296**: 673–677.
Shindell D, Rind D, Balachandran N, Lean J, Lonergan P. 1999. Solar cycle variability, ozone, and climate. *Science* **284**: 305.
Shindell DT, Schmidt GA, Mann ME, Rind D, Waple A. 2001. Solar forcing of regional climate change during the Maunder minimum. *Science* **294**: 2149–2152.
Smith TM, Reynolds RW, 2003. Extended reconstruction of global sea surface temperatures based on COADS data (1854–1997). *Journal of Climate* **16**: 1495–1510.
Sutton RT, Allen MR. 1997. Decadal predictability of North Atlantic sea surface temperature anomalies on the North Atlantic oscillation. *Journal of Climate* **13**: 122–138.
Thompson DWJ, Wallace JM. 1998. The Arctic oscillation signature in the wintertime geopotential height and temperature fields. *Geophysical Research Letters* **25**(9): 1297–1300.
Trenberth KE, Paolino Jr DA. 1980. The Northern Hemisphere sea-level pressure data set: trends, errors and discontinuities. *Monthly Weather Review* **108**: 855–872.
Von Storch HV, Zwiers FW. 1999. *Statistical Analysis in Climate Research*. Cambridge University Press.
Waple AM, Bradley RS. 1999. The sun–climate relationship in recent centuries: a review. *Progress in Physical Geography* **23**(3): 309–328.
White WB, Lean J, Cayan DR, Dettinger MD. 1997. Response of global upper ocean temperature to changing solar irradiance, *Journal of Geophysical*. *Research* **102**: 3255–3266.

